Region-of-Interest CT Reconstruction using One-Endpoint Hilbert Inversion in Optimized Directions

Aurélien Coussat, Simon Rit, Michel Defrise, Jean Michel Létang, Jean Michel Létang

Region-of-Interest CT Reconstruction using One-Endpoint Hilbert Inversion in Optimized Directions

Aurélien Coussat[1], Simon Rit[1], Michel Defrise[2], and Jean Michel Létang[1]

[1]Université de Lyon, INSA-Lyon, Université Claude Bernard Lyon 1, UJM-Saint Etienne, CNRS, Inserm, CREATIS UMR 5220, U1206, F-69373, Lyon, France
[2]Department of Nuclear Medicine, Vrije Universiteit Brussel, Brussels, Belgium

Abstract In computed tomography, scanning the entire object is sometimes impossible, causing truncated projection data. Reconstruction is however still possible: using differentiated backprojection, the Hilbert transform of the object can be calculated and inverted along line segments in the field-of-view. When two endpoints of the line segment are outside the object extent, a stable analytic reconstruction formula exists. When only one endpoint is outside the object extent, every pixel can be reconstructed, but no inversion formula is known yet. Uniqueness of the inverse Hilbert transform is nevertheless guaranteed along such segments, and a numerical inverse can be used. Most pixels of the field-of-view accept more than one "one-endpoint line segment" and one can choose the direction; we propose here to select the optimal direction based on an empirical criterion. Image quality improvement is assessed against a reconstruction that uses a single direction for every pixel.

1 Introduction

Conventional reconstruction procedures generally require the object to fit entirely within the scanner field-of-view (FOV), as they expect non-truncated tomographic data. However, in many imaging scenarios, such a condition cannot be met. Reconstruction must then use truncated projections. Recent theoretical results show that reconstruction is possible for some patterns of data truncation using, among other methods [1], the differentiated backprojection (DBP) followed by the inversion of the Hilbert transform. The reconstruction of some subset of the object, called region-of-interest (ROI), is then possible.

For simplicity, we focus on two-dimensional (2D) parallel beam tomography, although a generalization of the proposed method to three-dimensional cone-beam CT is possible. The source rotates along a 180° arc around the object. The scanner FOV is defined as the circular region where all points are illuminated by every source location. Knowledge of an approximate object extent Ω is assumed. If the FOV is entirely contained in the interior of Ω, then the problem is interior and will not be addressed in this work. We rather focus on the problem occurring when the FOV partly overlaps the object extent. The ROI is defined as this overlap: $\text{ROI} = \text{FOV} \cap \Omega$. Consider any line segment that overlaps Ω and whose two endpoints lie on the FOV border. The reconstructibility of this line segment varies depending on the number of its endpoints located inside Ω. When the two endpoints are located outside Ω, an analytic reconstruction formula can be applied [2]. When only one endpoint is located outside Ω, the line segment admits a unique and mathematically stable reconstruction [3], but no analytic formula is known yet. Unlike the "two-endpoint line segments", the "one-endpoint line segments" can reconstruct any pixel of the FOV. We refer to the problem of reconstructing such line segments as the "one-endpoint Hilbert inversion". This problem can be solved numerically by several techniques, such as projection onto convex sets [3] or singular value decomposition (SVD) [4, 5].

To our knowledge, the choice of a particular direction for the one-endpoint Hilbert line segment is a question that has never been addressed. In this work, each pixel of the image is reconstructed using a direction that seems optimal with respect to an empirical criterion. The reconstruction itself is achieved using extended SVD (XSVD) inversion [4]. A comparison with XSVD that uses a single Hilbert direction [4] is discussed.

2 Materials and Methods

Let $f : \mathbb{R}^2 \to \mathbb{R}$ be the sought object such that $\forall \boldsymbol{x} \notin \Omega, f(\boldsymbol{x}) = 0$. Let $p : [0;\pi[\times\mathbb{R} \to \mathbb{R}$ be the projections of f, corresponding to the scanner measurements, defined as

$$p(\phi, r) = p_\phi(r) = \int_{-\infty}^{+\infty} f\left(r\boldsymbol{\alpha}_\phi + s\boldsymbol{\beta}_\phi\right) \mathrm{d}s \qquad (1)$$

where $\boldsymbol{\alpha}_\phi = (\cos\phi, \sin\phi)$ and $\boldsymbol{\beta}_\phi = (-\sin\phi, \cos\phi)$. Since projections are truncated, $p(\phi, r)$ is unavailable for r below or above a certain threshold in some directions ϕ.

DBP links the projections to the sought object with

$$g_\theta(\boldsymbol{x}) = \frac{1}{2\pi} \int_\theta^{\theta+\pi} \left.\frac{\partial p(\phi, r)}{\partial r}\right|_{r=\boldsymbol{x}\cdot\boldsymbol{\alpha}_\phi} \mathrm{d}\phi = H_\theta f(\boldsymbol{x}) \qquad (2)$$

where H_θ is the one-dimensional Hilbert transform of a line of f in the direction $\theta \in [-\pi;\pi[$, defined as

$$H_\theta f(\boldsymbol{x}) = \fint_{-\infty}^{+\infty} \frac{f(\boldsymbol{x} - t\boldsymbol{\beta}_\theta)}{\pi t} \mathrm{d}t, \qquad (3)$$

$\boldsymbol{\beta}_\theta = (-\sin\theta, \cos\theta)$ and $\fint$ represents the Cauchy principal value of the integral [2]. Since the derivative is a local operation, the DBP is not impacted by projection truncation and yields the correct Hilbert transform of f for points measured by all projections, i.e., within the FOV. Therefore, f can be

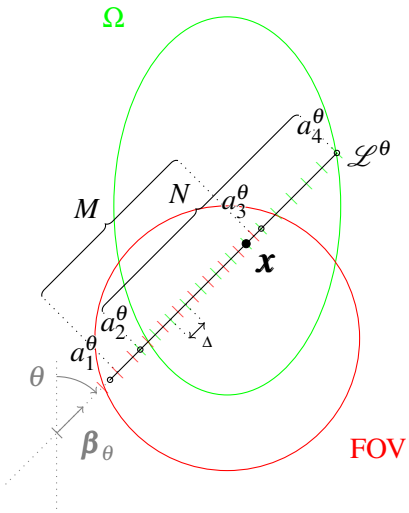

Figure 1: Notations employed in this work. The line segment $\mathscr{L}^\theta$ passes through the point $\boldsymbol{x}$ with an angle θ. The points $a^\theta_{1,\dots,4}$ are defined such that the data are measured on the segment $[a_1^\theta, a_3^\theta]$, and the object extent Ω is included in segment $[a_2^\theta, a_4^\theta]$. The samples of $\boldsymbol{g}$ are illustrated as the red ticks, and the samples of $\boldsymbol{f}$ as the green ticks.

reconstructed inside the FOV by applying an inverse truncated Hilbert transform to the DBP over enough segments to cover the FOV.

We now focus on the reconstruction of a single pixel $\boldsymbol{x} \in$ ROI, and we omit the $\boldsymbol{x}$ dependency of all symbols defined below for clarity. Let $\mathscr{L}^\theta$ be a one-endpoint line segment that passes through $\boldsymbol{x}$ at some angle θ, and let $\Delta > 0$ be the sampling step along $\mathscr{L}^\theta$. We define $\boldsymbol{g} \in \mathbb{R}^M$ as the vector whose components are defined as

$$g_{i-a_1^\theta+1} = g_\theta\left(\boldsymbol{x} + \left(i - \frac{1}{2}\right)\Delta\boldsymbol{\beta}_\theta\right) \quad \text{for} \quad a_1^\theta \le i \le a_3^\theta \quad (4)$$

with $M = a_3^\theta - a_1^\theta + 1$. The integers $(a_1^\theta, a_3^\theta) \in \mathbb{Z}^2$ are chosen such that $\boldsymbol{g}$ samples the entire FOV along $\mathscr{L}^\theta$.

Similarly, the vector $\boldsymbol{f} \in \mathbb{R}^N$ has its components defined as

$$f_{j-a_2^\theta+1} = f\left(\boldsymbol{x} + j\Delta\boldsymbol{\beta}_\theta\right) \quad \text{for} \quad a_2^\theta \le j \le a_4^\theta \quad (5)$$

with $N = a_4^\theta - a_2^\theta + 1$. The integers $(a_2^\theta, a_4^\theta) \in \mathbb{Z}^2$ are chosen such that $\boldsymbol{f}$ entirely bounds Ω along $\mathscr{L}^\theta$. Note that the integers $a^\theta_{1,\dots,4}$ depend on $\boldsymbol{x}$ and θ since the distances between the FOV borders, Ω borders and $\boldsymbol{x}$ vary with θ. The sought value at $\boldsymbol{x}$ corresponds to Equation (5) with $j = 0$; we thus have $a_1^\theta < a_2^\theta < 0 < a_3^\theta < a_4^\theta$. If these inequalities do not hold, then $\mathscr{L}^\theta$ is not one-endpoint. Figure 1 summarizes these notations.

As shown in Equation (2), the link between $\boldsymbol{f}$ and $\boldsymbol{g}$ is the Hilbert transform, which, in its discrete form, can be expressed as $\mathbf{H}$, an $M \times N$ matrix whose values are defined as

$$H_{i-a_1^\theta+1, j-a_2^\theta+1} = \frac{1}{\pi}\frac{1}{i-j-\frac{1}{2}} \quad \text{for} \quad \begin{cases} a_1^\theta \le i \le a_3^\theta \\ a_2^\theta \le j \le a_4^\theta \end{cases} \quad (6)$$

such that $\mathbf{H}\boldsymbol{f} = \boldsymbol{g}$. The θ dependency of $\boldsymbol{f}$, $\boldsymbol{g}$ and $\mathbf{H}$ has been omitted for clarity. Note the term $-\frac{1}{2}$ appearing in Equations (4) and (6): this half-pixel shift improves the reconstruction resolution [6]. We used here the XSVD procedure, based on truncated SVD, to reconstruct $\boldsymbol{f}^{\text{XSVD}}$ [4]. The value at $\boldsymbol{x}$ is then $f^{\text{XSVD}}_{-a_2^\theta+1}$, i.e. Equation (5) for $j = 0$.

Any angle θ such that $\mathscr{L}^\theta$ is a one-endpoint line segment theoretically works to apply the reconstruction procedure. Note that points having a two-endpoint line segment should be reconstructed using the analytic formula [2], but we force here the usage of one-endpoint line segments for simplicity and to better evaluate the proposed method. We have previously observed a residual artifact with XSVD and that some Hilbert directions give better results than others. We therefore propose to select the direction that minimizes some criterion $\mathscr{C}$ for a given point $\boldsymbol{x}$ depending on the problem parameters $a^\theta_{1,\dots,4}$, that is

$$\hat{\theta} = \arg\min_\theta \mathscr{C}\left(a_1^\theta, a_2^\theta, a_3^\theta, a_4^\theta\right). \quad (7)$$

Two different criteria were considered in this study. We first empirically decided to minimize the distance between a_3^θ and a_4^θ, as it is the part of the segment that cannot be reconstructed, relatively to the number of values $a_3^\theta - a_2^\theta$ that can be reconstructed. This criterion is modeled as

$$\mathscr{C}_1\left(a_1^\theta, a_2^\theta, a_3^\theta, a_4^\theta\right) = \frac{a_4^\theta - a_3^\theta}{a_3^\theta - a_2^\theta}. \quad (8)$$

A known artifact of XSVD reconstructions is an offset whose intensity decreases with the distance to the inner FOV border [4]. We designed another criterion aiming at maximizing the distance between $\boldsymbol{x}$ and the FOV boundary in the direction θ. This second criterion is expressed as

$$\mathscr{C}_2\left(a_1^\theta, a_2^\theta, a_3^\theta, a_4^\theta\right) = -a_3^\theta. \quad (9)$$

The proposed method was evaluated using computer simulations of the 2D Shepp-Logan phantom scaled up 96 times. A set of 720 parallel projections of 800 rays each were analytically computed over an arc of 180°. The pixel spacing of the projections was 0.25 mm. Reconstructions were computed on a 256×256 pixel grid, in which only the pixels within the FOV were reconstructed. A FOV was simulated by using the DBP data only from inside a circular region located near the bottom of the phantom. The estimated object extent is an ellipse that encompasses the phantom with a 1 % margin. The sampling step Δ was set to 0.25 mm. The resulting setup is as in Figure 1. The pixel spacing of the reconstruction was 1 mm. For comparison, the same reconstruction was performed with the Hilbert direction θ set to 0 (vertical) for all pixels.

For each pixel of the ROI and for a given angle θ, our implementation analytically computes the locations of the intersections between the segment and the FOV or Ω. The

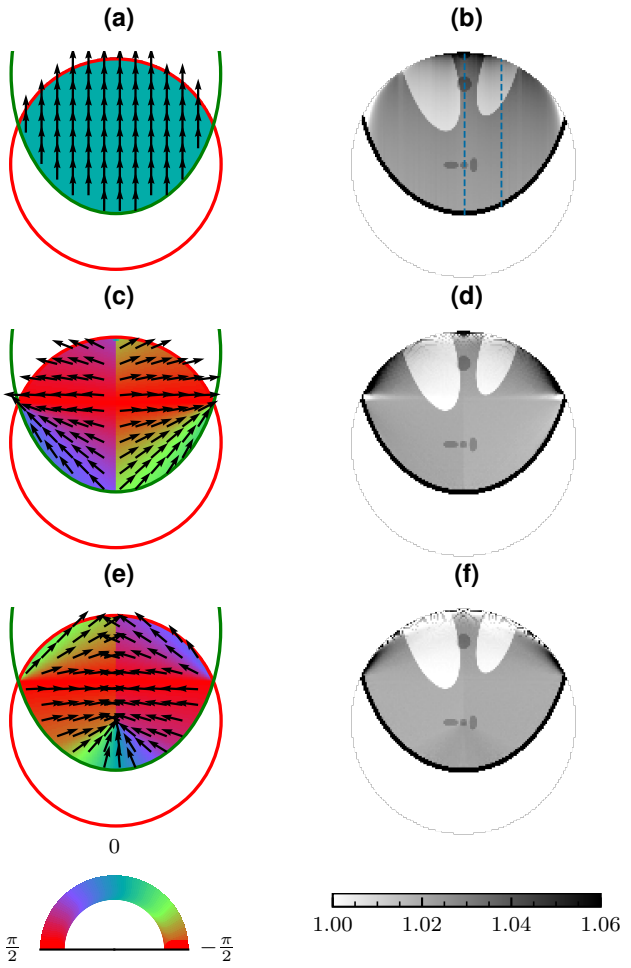

Figure 2: (a) and (b): directions and reconstruction when all directions are vertical. (c) and (d): directions and reconstruction for criterion $\mathscr{C}_1$. (e) and (f): directions and reconstruction for criterion $\mathscr{C}_2$.

optimization problem of Equation (7) is solved numerically by evaluating its right-hand side for every value of θ with a 0.25° step. Then, the DBP is computed on every sample of $\boldsymbol{g}$ to apply the XSVD. All simulations were implemented using Python 3.8.5, NumPy 1.19.4 and RTK 2.1.0 [7].

3 Results

Figure 2 shows directions and reconstructed images using either a vertical direction for every pixel (Figures 2a and 2b), the criterion $\mathscr{C}_1$ (Figures 2c and 2d) or the criterion $\mathscr{C}_2$ (Figures 2e and 2f).
Figure 3 shows profiles through two columns of the reconstructed images displayed in Figures 2b, 2d and 2f. Figure 3a shows the central column; Figure 3b shows the column located at 22 mm on the right hand side of the FOV center. The profile locations are displayed in Figure 2b.

4 Discussion

Using a single Hilbert direction aligned to the pixel grid to reconstruct the entire FOV has some advantages: a single inversion is sufficient to reconstruct a whole line of pixels, and the procedure is computationally inexpensive. However, it also has major drawbacks: a single direction is not enough for a full-FOV reconstruction in many configurations, and the chosen direction can be sub-optimal for some pixels, deteriorating the reconstruction. This procedure was reproduced and the result is shown in Figure 2b. This reconstruction also displays slight vertical streaks in the Hilbert direction because each line is treated as an independent problem. The method proposed here avoids these limitations, because each pixel is treated as an independent problem.
Figures 2d and 2f show that the reconstructions are less accurate than that of Figure 2b for pixels lying close to the FOV inner boundary. This poor quality is probably due to the interpolation used to compute the DBP in Figures 2d and 2f, whereas Figure 2b uses exact values, as it is less computationally demanding to do so in a single Hilbert direction. However, in the rest of the ROI, the quality is higher by the use of multiple Hilbert directions; this improvement is visible on Figure 3. The discretization of the angle θ, when solving Equation (7), may explain the small streak artifacts visible in the reconstructions.
The pixels close to the interior endpoint are known to be difficult to reconstruct. We attribute this difficulty to the decreasing numerical stability of the one-endpoint Hilbert inversion model [3]. The same instability was observed in previous works performing one-endpoint reconstructions using XSVD [4, 5], where it was shown that this instability creates an offset whose intensity increases towards the interior endpoint. On Figure 3, this effect is clearly visible, especially looking at the profile of the reconstruction shown in Figure 2b; the same offset, although not as intense, is observed when each pixel uses its own direction. Interestingly, the offset is also observed in other works not using SVD inversion [3, 8–10], suggesting that this effect is not directly caused by the one-endpoint Hilbert inversion but is instead intrinsic to the ROI tomography problem.
As an attempt to reduce this offset, the criterion $\mathscr{C}_2$ (Equation (9)) was designed to favor directions that maximize the distance between the FOV border and the sought pixel. Figure 3 illustrates the improvements yielded by $\mathscr{C}_2$: the offset is considerably reduced compared to that of a reconstruction performed in a fixed direction. Figure 2e shows that the bottom of Ω is reconstructed using almost vertical directions using this criterion; this observation explains the similar quality to that of the vertical-only reconstruction, as shown on the left side of Figure 3a. Criterion $\mathscr{C}_1$ also diminishes the offset, but two areas near the intersections between the FOV and Ω, visible in Figure 2d, are reconstructed with a poor quality. Neither $\mathscr{C}_1$ nor $\mathscr{C}_2$ stands out and the optimal criterion remains to be found.
The line that connects the two intersection points between Ω and the FOV boundaries forms a border between two regions. Pixels located above this border are only crossed by line segments that are at most one-endpoint, which fits

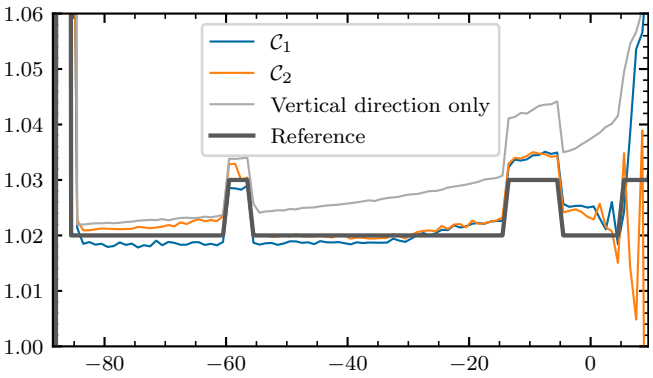

(a) Profile through the central column.

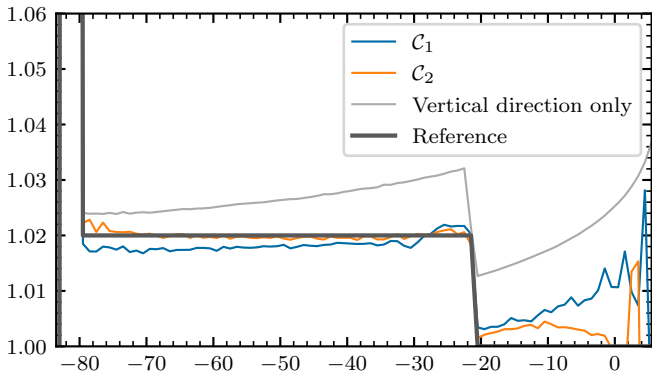

(b) Profile through the column located at 22 mm on the right hand side of the FOV center.

Figure 3: Two vertical profiles, shown in Figure 2b, of the reconstructions displayed in Figures 2b, 2d and 2f. The x-axis is limited to the ROI; the y-axis is limited to the grayscale limit $[1; 1.06]$.

the proposed approach. On the other hand, pixels that lie below the line accept at least one two-endpoint segment; along these segments, an analytic inversion formula should instead be applied [2] since this two-endpoint inversion is more accurate than the one-endpoint inversion. However, full-FOV reconstruction is impossible using two-endpoint line segments only. A previous work explored the possibility of combining two- and one-endpoint reconstructions in a single image [5]; here, for simplicity and to better evaluate the proposed method, the full FOV is reconstructed using one-endpoint line segments only, although it is not optimal.

5 Conclusion

We have proposed a method for ROI reconstruction from truncated projections using one-endpoint Hilbert inversion techniques. This method selects a different Hilbert direction for each pixel, chosen to optimize some criterion; here, we empirically designed two criteria. The proposed method is able to reconstruct any non-interior ROI tomography problem, while maintaining a satisfactory image quality. Noteworthy improvements were observed compared to a similar method that uses a fixed Hilbert direction for all pixels.

Acknowledgments

This work was supported by grant ANR-17-CE19-0006 (ROIdoré project) from the Agence Nationale de la Recherche (France). This work was performed within the framework of the SIRIC LYriCAN Grant INCa_INSERM_DGOS_12563 and of the LABEX PRIMES (ANR-11-LABX-0063) of Université de Lyon, within the program 'Investissements d'Avenir' (ANR-11-IDEX-0007) operated by the French National Research Agency (ANR).

References

[1] R. Clackdoyle and M. Defrise. "Tomographic Reconstruction in the 21st Century". *IEEE Signal Processing Magazine* 27.4 (July 2010), pp. 60–80. DOI: 10.1109/MSP.2010.936743.

[2] F. Noo, R. Clackdoyle, and J. Pack. "A Two-Step Hilbert Transform Method for 2D Image Reconstruction". *Physics in Medicine and Biology* 49.17 (Sept. 2004), pp. 3903–3923. DOI: 10.1088/0031-9155/49/17/006.

[3] M. Defrise, F. Noo, R. Clackdoyle, et al. "Truncated Hilbert Transform and Image Reconstruction from Limited Tomographic Data". *Inverse Problems* 22.3 (June 2006), pp. 1037–1053. DOI: 10.1088/0266-5611/22/3/019.

[4] A. Coussat, S. Rit, R. Clackdoyle, et al. "Region-of-Interest CT Reconstruction Using Object Extent and Singular Value Decomposition". *IEEE Transactions on Radiation and Plasma Medical Sciences* (2021). DOI: 10.1109/TRPMS.2021.3091288.

[5] A. Coussat, S. Rit, R. Clackdoyle, et al. "ROI CT Reconstruction Combining Analytic Inversion of the Finite Hilbert Transform and SVD". *CT Meeting* (July 2020), p. 4.

[6] F. Noo, J. Pack, and D. Heuscher. "Exact Helical Reconstruction Using Native Cone-Beam Geometries". *Physics in Medicine and Biology* 48.23 (Dec. 2003), pp. 3787–3818. DOI: 10.1088/0031-9155/48/23/001.

[7] S. Rit, M. Vila Oliva, S. Brousmiche, et al. "The Reconstruction Toolkit (RTK), an Open-Source Cone-Beam CT Reconstruction Toolkit Based on the Insight Toolkit (ITK)". *Journal of Physics: Conference Series* 489 (Mar. 2014), p. 012079. DOI: 10.1088/1742-6596/489/1/012079.

[8] R. Clackdoyle, F. Noo, J. Guo, et al. "Quantitative Reconstruction from Truncated Projections in Classical Tomography". *IEEE Transactions on Nuclear Science* 51.5 (Oct. 2004), pp. 2570–2578. DOI: 10.1109/TNS.2004.835781.

[9] E. Rashed, H. Kudo, and F. Noo. "Iterative Region-of-Interest Reconstruction From Truncated CT Projection Data Under Blind Object Support". *Medical Imaging Technology*. 5th ser. 27 (Nov. 2009), pp. 321–331. DOI: 10.11409/mit.27.321.

[10] R. Clackdoyle, F. Noo, F. Momey, et al. "Accurate Transaxial Region-of-Interest Reconstruction in Helical CT?" *IEEE Transactions on Radiation and Plasma Medical Sciences* 1.4 (July 2017), pp. 334–345. DOI: 10.1109/TRPMS.2017.2706196.